catalysts

MDPI

Article

Innovative Synthetic Approaches for Sulphate-Promoted Catalysts for Biomass Valorisation

Alessia Giordana [1], Cristina Pizzolitto [2], Elena Ghedini [2], Michela Signoretto [2], Lorenza Operti [1] and Giuseppina Cerrato [1,*]

[1] Dipartimento di Chimica, Università di Torino, 10125 Torino, Italy; alessia.giordana@unito.it (A.G.); lorenza.operti@unito.it (L.O.)
[2] Dipartimento di Scienze Molecolari e Nanosistemi, Università "Ca' Foscari" Venezia, 30172 Venezia, Italy; cristinapizzolitto@hotmail.it (C.P.); elena.ghedini@unive.it (E.G.); miky@unive.it (M.S.)
* Correspondence: giuseppina.cerrato@unito.it

Abstract: In the present research, we report on an innovative and quick procedure for the synthesis of metal oxides: a sol-gel procedure which is followed by two steps that are assisted by microwaves (MW) heating. First, MW heating promotes gel drying and successively permits the calcination of the xerogel in a few minutes, using a susceptor that rapidly reaches high temperatures. The procedure was employed for the synthesis of zirconium dioxide (ZrO_2), and MW-assisted calcination enables the collection of tetragonal ZrO_2, as confirmed by different experimental techniques (PXRD, HR-TEM and Raman spectroscopy). Using this MW-assisted sol-gel procedure, a promoted sulphated zirconia (SZ) has been obtained. Both the nature and strength of SZ surface acidity have been investigated with FTIR spectroscopy using CO and 2,6-dimethylpyridine (2,6-DMP) as probe molecules. The obtained materials were tested as catalysts in acid hydrolysis of glucose to give 5-(hydroxymethyl)furfural (5-HMF). One of the obtained catalysts exhibited a better selectivity towards 5-HMF with respect to SZ material prepared by a classical precipitation route, suggesting that this procedure could be employed to obtain a well-known catalyst with a less energy-consuming procedure. Catalytic results also suggest that good selectivity to 5-HMF can be achieved in aqueous media in the presence of weak Lewis and Brønsted sites.

Keywords: HMF; solid acid catalyst; biomass valorization; Lewis/Brønsted acidity; sulphated zirconia; MW synthesis; IR spectroscopy

check for updates

Citation: Giordana, A.; Pizzolitto, C.; Ghedini, E.; Signoretto, M.; Operti, L.; Cerrato, G. Innovative Synthetic Approaches for Sulphate-Promoted Catalysts for Biomass Valorisation. *Catalysts* **2023**, *13*, 1094. https://doi.org/10.3390/catal13071094

Academic Editors: Orhan Şişman, Surjyakanta Rana, José Joaquín Velázquez García and Rajesh Dagupati

Received: 14 June 2023
Revised: 6 July 2023
Accepted: 10 July 2023
Published: 12 July 2023

Copyright: © 2023 by the authors. Licensee MDPI, Basel, Switzerland. This article is an open access article distributed under the terms and conditions of the Creative Commons Attribution (CC BY) license (https://creativecommons.org/licenses/by/4.0/).

1. Introduction

Catalytic systems based on sulphated zirconia (SZ) have attracted extensive attention since their first discovery due to their apparently unusual acidic properties and high activity in light *n*-alkanes conversion in mild conditions [1]. In the late 1990s of the 20th century, much work was devoted to the study of syntheses, surface characterisation, and possible applications of these catalytic materials. In particular, it was reported that acidic and catalytic properties of SZ-based catalysts might depend on a very high number of preparative parameters [2,3], among which of particular relevance are (i) sulphation procedure [4], (ii) calcination temperature, and (iii) activation conditions [5]. Generally speaking, a necessary structural condition to obtain SZ systems catalytically active in the isomerisation reaction of light *n*-alkanes seems to be the presence of a stable tetragonal zirconia phase (t-ZrO_2). It was seldom claimed that sulphation of the more thermodynamically stable monoclinic zirconia phase (m-ZrO_2) might lead to catalytic performances comparable to those of sulphated t-ZrO2 (see, for instance, [6]). Moreover, as far as the ZrO_2 polymorph is concerned, the catalytic activity of a cubic SZ system turns out to be by far the highest one when compared to either the monoclinic or tetragonal phases that have been examined [7].

More recently, in order to spread the possible use of ZrO_2 to other catalytic applications and simultaneously to "open the door" to environmentally friendly preparation routes, the

research has been focused on (i) microwave- (MW) and (ii) ultrasounds-assisted procedures or to (iii) "greener" solvents employment [8]. All of these new approaches have also brought about the use of zirconia, either as such, as support for metallic nanoparticles (NPs), or to be embedded into mesoporous systems (e.g., SBA-15) in different catalytic routes for biomass conversion [3,9,10].

Biomass represents a renewable source of organic molecules for the manufacturing of chemicals and fuels (which are mainly derived from petrol nowadays), which can be converted into platform molecules—building blocks that can be converted to a wide range of chemicals or materials such as 5-hydroxymethylfurfural (5-HMF) and levulinic acid (LA) [11]. Biomass conversion is often governed by carbocation chemistry, which requires acidic active sites on the catalysts. SZ-based material presents both Lewis (L) and Brønsted (B) acid sites since they are potential catalysts in glucose hydrolysis. This reaction is consecutive and involves various steps: it is supposed to start via isomerisation to fructose and continue through dehydration to 5-HMF, which could then possibly be hydrolysed into LA (see Scheme 1). The first step is supposed to be L acid-catalysed, while dehydration/hydration reactions are catalysed by L and B acid sites. The presence of B acidity facilities the rehydration of 5-HMF but is responsible for retarding the isomerisation and promoting the condensation reactions, forming humins [12]. To enhance 5-HMF selectivity, it is necessary to control the B and L acid sites' proportion but also to tune their strength [13]. In fact, it has been supposed that weak L acid sites could promote the formation of 5-HMF, whereas medium-to-strong L acid sites affect 5-HMF yield for the formation of LA and/or undesired humins. B acid sites not only have a detrimental effect on glucose conversion but also promote aldol addition and condensation reactions from 5-HMF. The poor stability of 5-HMF in acid-aqueous solutions could also lead to low selectivity and difficulties in isolation, so different solvents (DMSO, ionic liquid) and biphasic systems have also been proposed to improve yields [14,15]. The nature of the surface catalyst is very important to tune selectivity; a comprehensive DFT study suggests that the final product from glucose dehydration is determined by which hydroxyl group is protonated first [16]. In this respect, for SZ, an appropriate mix of L and B sites is required for the tandem isomerisation of glucose to fructose and its subsequent dehydration to 5-HMF. In the literature, it is reported that m-ZrO_2, possessing only L sites, is effective for glucose isomerisation to fructose but poorly active towards fructose dehydration to 5-HMF, while using SZ, possessing B acidity, the 5-HMF production is enhanced [17].

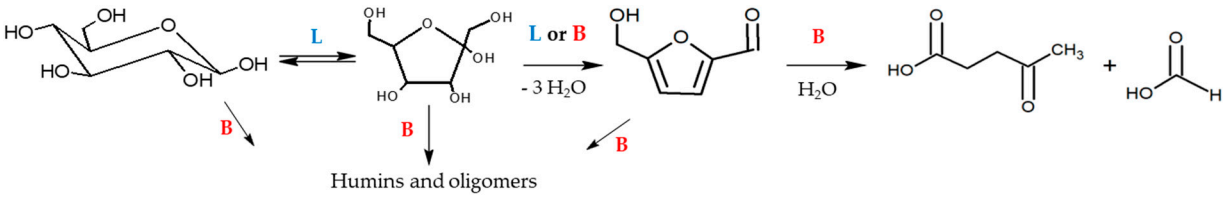

Scheme 1. Reaction mechanism for glucose acid hydrolysis.

Getting back to possible alternative preparative routes, MW-assisted methods have been applied to the synthesis of inorganic material and can help in overcoming the disadvantages of common synthetic techniques (i) by reducing reaction time, (ii) improving yield, and (iii) leading to the obtainment of nanoparticles with homogenous distribution of both shape and dimensions [18–21]. Some studies can be found in the literature on zirconia-based materials synthesis [8]. Cubic ZrO_2 has been obtained by combustion promoted by MW heating [22]. ZrO_2 NPs, generally possessing a tetragonal phase, have been obtained by MW-hydrothermal treatment using different precursors [23–26] and by sol-gel synthesis assisted by MW irradiation. For example, Fetter et al. [27] reported the synthesis of ZrO_2 and Cu/ZrO_2 starting from zirconium butoxide and operating at different pH values. Gel formation was induced by MW irradiation, and the obtained powder was then calcined at 600 °C. They reported that the powder always crystallised in the tetragonal

phase. Dwivedi et al. [28] applied the MW-assisted citrate sol-gel method to obtain zirconia. The gel was dried under MW irradiation and then subsequently calcined at 450 °C. Also, in this case, the formation of t-ZrO_2 was observed. Silva et al. [29] reported the preparation of pristine and Gd-doped ZrO_2 by a two-step synthetic route, both assisted by MW irradiation. The first step involved gel formation, while in the second step, the obtained product was calcined by an MW hybrid method. Their results suggest that MW heating enhanced the formation of the tetragonal phase.

In this work, we propose an MW-assisted sol-gel procedure for ZrO_2 synthesis that involves two MW-assisted steps. In the former, the gel is dried under MW irradiation, whereas in the latter, the obtained xerogel is calcinated by an MW hybrid method. The MW hybrid heating method, which employs a susceptor that transfers heat to the sample, has been previously applied in materials production, ceramic sintering, and solid-state syntheses of mixed oxides [30,31]. However, to the best of our knowledge, this hybrid procedure has never been considered to carry out calcination on amorphous materials. Then the procedure was applied to the synthesis of SZ powder, a well-known, solid acid catalyst, investigating the effect of the sulphate addition step and the impregnation method on the nature of sulphate surface sites of the obtained materials. Finally, the materials have been tested as catalysts in glucose hydrolysis for 5-HMF production by trying to correlate selectivity to L and B surface acidity. This last step of characterisation has been studied by means of FT-IR spectroscopy, using carbon monoxide (CO) and 2,6-dimethylpyridine (2,6-DMP) as probe molecules.

2. Results and Discussion

2.1. MW-Assisted Synthesis of ZrO_2

The proposed MW-assisted procedure for the synthesis of zirconia can be divided into three steps: (i) gel formation, (ii) MW-assisted drying, and (iii) MW-assisted calcination. Many parameters could influence the MW treatments. To ensure the reproducibility the same vessels (positioned in the focusing position of the oven) and the same volume of samples were used for each specific treatment in the MW oven. Different trials were attempted to test and optimise the procedure in MW-assisted steps and to find the most appropriate power level in each step as well. To go into further details of the procedure, we report on the following synthesis of sample Z1 (obtained using HNO_3 as catalysts in gel formation). In the first step, the gel was quickly formed at ambient temperature. Then, in the MW-assisted drying, the liquid phase was eliminated from the gel by evaporation promoted by a few minutes of MW irradiation. A Raman spectrum of the liquid collected after evaporation (blue curve in Figure 1a) exhibits signals attributable to the ν_{10} mode of 1-propanol, from zirconium precursor, and ethanol, used as a solvent (respectively, at 861 and 885 cm^{-1}) [32]. PXRD analysis evidenced that after MW-assisted drying, the powder is still amorphous. Comparing Raman spectra of xerogel and gel (black and green curves in Figure 1a), we can appreciate the disappearance of signals assigned, respectively, to the ν_{10} mode of alcoholic solvents and the stretching modes of C–H (around 3000 cm^{-1}), confirming that the majority of the liquid phase has been removed. Xerogel is supposed to be formed by zirconium oxy-hydroxide, as suggested by both the broad peak at 450 cm^{-1} and the signals located below 1000 cm^{-1}, ascribable to Zr–O modes [33,34]. The intense band at 1050 cm^{-1} can be ascribed either to the symmetric vibration of the nitrate ions or to a vibration of the Zr–OH group [35]. The product obtained by MW-assisted drying exhibits no heating when exposed to MW; even when using the maximum power and a long exposure time, no changes are observed in the material, so it is MW-transparent. Thus, we decided to employ a second MW-adsorbing material or susceptor (as SiC, carbon materials and CuO), which was rapidly heated by MW to reach a high T quickly. We used graphite as a susceptor [31,32], which allowed us to quickly reach T in the 450 and 750 °C range (as measured using an optic pyrometer and a thermocouple, detailed in SI). MW-assisted calcination permits the obtainment, after a few minutes of treatment, of a white powder named sample Z1. A Raman spectrum of Z1 (red curve in Figure 1a) exhibits the

pattern of t-ZrO_2 with characteristic signals at 149, 271, 317, 461, 602, and 646 cm^{-1} [7,34]. PXRD confirms the formation of pure t-ZrO_2 (see Figure S1). HR-TEM images indicate the presence of NPs with dimensions around 10 nm (in Figure 1b), showing small and homogeneous crystallites having roundish contours with closely packed features. NPs present a highly ordered habit, as it is quite simple to single out fringe patterns confirming the high crystallinity of the Z1 sample. The detailed inspections of the distances of the fringe patterns and the parallel analysis of the diffraction patterns (see the inset of Figure 1c) indicate that the most frequently observed fringe patterns belong to either (101) and (112) family planes of t-ZrO_2.

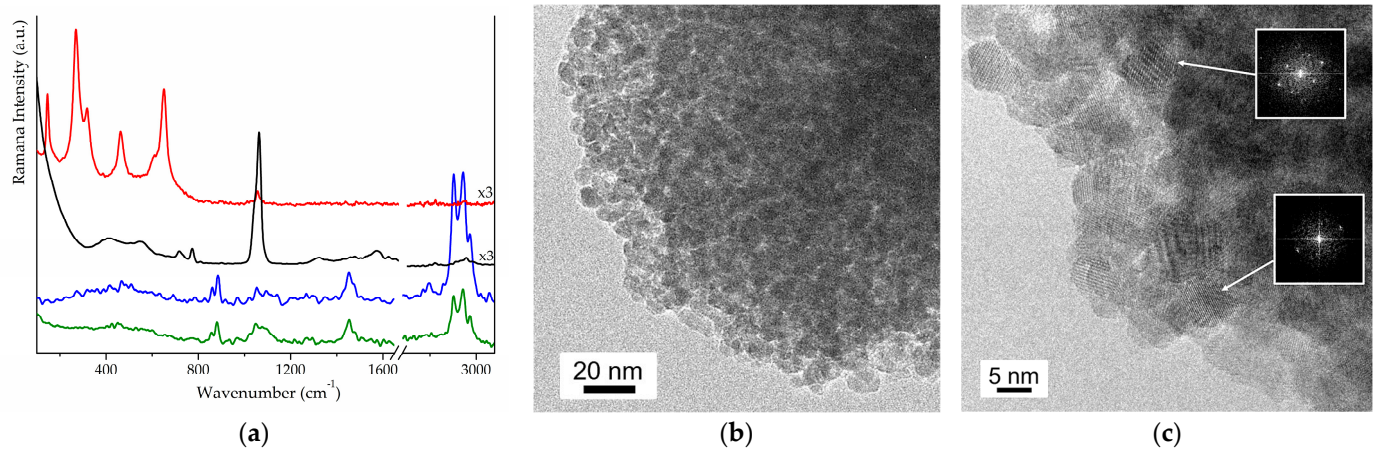

(**a**) (**b**) (**c**)

Figure 1. (**a**) Raman spectra of intermediates and product in the synthesis of Z1: gel in green, the liquid removed from the gel in blue, the obtained xerogel in black and the product obtained by MW-calcination in red; (**b**,**c**) HR-TEM images of Z1 and simulated (FFT) electronic diffraction of (101) and (112) family planes with d_{hkl} of 0.299 and 0.183 nm, respectively, in the inset (ICCD PDF card n. 01–088-1007).

Using the same procedure, we try to employ sulfuric and acetic acid as hydrolysis catalysts. ATR and PXRD data indicate that the obtained xerogels have characteristics similar to that of Z1 material: they are amorphous and composed of zirconium oxyhydroxide. Both products remain amorphous after MW-assisted calcination, even increasing both the time and power levels of MW irradiation (as shown in Figure S1). It is interesting to notice that, unlike with Z1, signals ascribable to the anions coming from the acid medium are still present after MW-calcination, as evidenced by ATR spectroscopy (as shown in Figure S2). These results suggest that there is an influence of the ion in the calcination step: nitrate ions are easily eliminated under the rapid heat treatment; on the contrary, acetate and sulphate ions remain in the powder and seem to inhibit the crystallisation process.

To understand which step is more influenced by MW irradiation, we decided to prepare samples subjected to only one MW treatment. Sample Z2 was obtained from a xerogel (synthesised by MW-assisted drying) calcined in a muffle at 450 °C for 1 h. Sample Z3 was obtained by MW-assisted calcination of zirconium oxy-hydroxide intermediate (obtained by precipitation from $ZrOCl_2$). PXRD of Z2 and Z3 (reported in Figure S1) indicate the formation of t-ZrO_2 (ICCD PDF card n. 01–088-1007), and only for Z2 the presence of a small fraction of the monoclinic phases (Vm = 0.11 and 0.14 by PXRD and Raman data, respectively). We can also observe that peaks are broader in the Z3 diffractogram, indicating that crystallites are very small, even smaller than the Z1 ones. These results suggest that MW-assisted calcination is the most effective step, affecting to a very large extent the formation of a tetragonal phase, probably due to the rapid heating that seems to favour nucleation, growth, and stabilisation of small particles.

2.2. MW-Assisted Synthesis of SZ Powders

The proposed procedure allows us to obtain t-ZrO_2 (the crystalline phase reported to have superior catalytic activity), so we decided to apply the MW-assisted procedure to the synthesis of SZ, a well-known solid acid catalyst [2,10,36,37]. Sulphates were added starting from $(NH_4)_2SO_4$, chosen because thermal de-ammonium is reported to start around 200–250 °C [38,39], and so ammonium can be easily eliminated in MW-calcination. Sulphates were added by either wetness impregnation (WI) or incipient wetness impregnation (IWI) on (i) xerogel or on (ii) the already formed t-ZrO_2 (respectively, indicated as S1Z and S2Z). In both cases, after impregnation, dried powders were calcined by MW-assisted procedure.

Structural and vibrational characterisations of samples obtained by WI are reported in Figure 2a. Raman spectra exhibit the typical pattern of t-ZrO_2 [7,40], but for S2Z_WI, it is also possible to recognise the most intense signals of the monoclinic phase (at 175, 186, 376 cm^{-1}) [40], which were absent before sulphation. PXRD data confirmed that sulphation on S2Z_WI induces modification on its crystal phase (Vm = 0.04), while the lower intensity in S1Z_WI peaks indicates a minor grade of crystallinity. In fact, Raman signals possess very low intensity for S1Z_WI—a broad band above 1000 cm^{-1} is now evident, and it is supposed to be associated with surface sulphates that have a more ionic character.

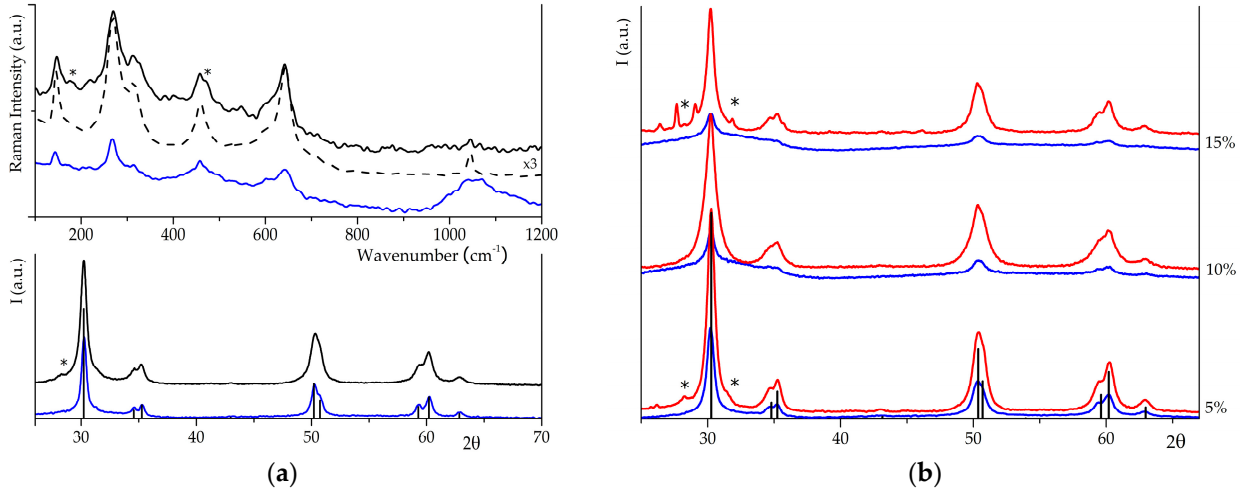

Figure 2. (**a**) Raman spectra and diffractograms of S1Z_WI (in blue) and S2Z_WI (in black), dotted line for intermediate ZrO_2, before impregnation; (**b**) Diffractograms of S1Z (in blue) and S2Z (in red), impregnated by IWI with sulphates at increasing wt%. Bars indicate reference patterns of t-ZrO_2 (ICCD PDF card n. 01-088-1007), and stars (*) indicate monoclinic signals (ICCD PDF card n. 037-1484).

Sulphates were added by IWI in different synthetic steps at increasing wt%. When IWI was carried out on xerogel (S1Z), the structural characterisation indicates that the material exhibited a partially amorphous structure as far as the amount of nominal sulphates increased. As evident in Figure 2b, peaks present in the S1Z_5 diffractogram indicate the formation of the tetragonal phase, whereas, for S1Z_10 and S1Z_15, the presence of a still amorphous fraction is suggested by both the lower intensity of the peaks and the broadening at around 30°. When IWI was carried out on t-ZrO_2 (S2Z), the resulting materials were crystalline, exhibiting the typical XRD pattern of the tetragonal phase, as evidenced in Figure 2b. S2Z_5 and S2Z_15 exhibit a small fraction of the monoclinic phase. Raman data (see Figure S3) confirm the previous assumptions. S1Z_5 curve exhibits the pattern of t-ZrO_2 [7], and S1Z_10 and S1Z_15 spectra are very similar to those reported for amorphous zirconia. The broad signal at 1050 cm^{-1} exhibited by all S1Z samples could be related to ionic sulphate groups. Curves of S2Z samples exhibit the pattern of t-ZrO_2 [7], but signals of the monoclinic phase are less evident. So, we can preliminarily conclude that (i) the crystallinity of the final products strongly depends on the impregnation step,

independently of the employed impregnation method, and (ii) MW-assisted calcination is less effective if it is carried out on the impregnated amorphous intermediate.

Raman spectra suggest that S1Z samples present sulphates with ionic character, but the nature of surface sulphates is better investigated by means of IR spectroscopy. ATR spectra (see Figure S4) of S1Z samples exhibit a broad band in the 1250–900 cm^{-1} range. These spectra are similar to that of $Zr(SO_4)_2$ [41], suggesting an ionic nature of sulphates on S1Z samples, further supported by band broadening. For S1Z_5, the band is more structured, suggesting that at lower concentrations, sulphates reach, almost in part, a covalent character. In the ATR spectra of S2Z, the peak located at 1423 cm^{-1} is ascribable to the asymmetric stretching mode of the S=O bond of polynuclear sulphates as indicated in the literature [42], and the broad band at lower wavenumbers is ascribable to the stretching mode of S–O [43,44]. The presence of these signals suggests a covalent character of sulphate groups for S2Z_WI, S2Z_5 and S2Z_10. Only when sulphation is carried out on the t-ZrO_2, covalent sulphate species are present at the surface of the obtained materials.

2.3. SZ as Catalyst for Biomass Valorization

SZ powders were tested as catalysts in glucose hydrolysis to produce platform chemicals, as either 5-HMF or LA. It is widely accepted that the reaction is consecutive and involves various steps, catalysed by either L or B acidic sites present at the surface of the solid catalyst, and the reaction pathways for 5-HMF and LA are quite similar. As discussed above, the reaction pathway and selectivity depend on the strength and ratio of L and B acid sites [12,13]. In SZ catalysts, L and B acidity is related to both nature and the amount of sulphate ions. The nature of surface sulphates, and nature and the strength of surface acidity as well, is influenced by the preparation method. We tested three SZ samples obtained by impregnation in different synthetic steps and a 'model' system: (i) S2Z_WI (by WI on t-ZrO_2), (ii) S1Z_5 (by IWI on xerogel), (iii) S2Z_8 (by IWI on t-ZrO_2) and (iv) SZ_p, a 'model' SZ system obtained by a standard precipitation route [1,2,37], as indicated in Table 1. All these samples consist of SZ NPs possessing tetragonal phase, and FT-ATR analyses on the employed catalysts, described in Section 2.2, suggest that these materials possess surface sulphates with different natures (covalent and ionic), leading to surface acid sites of different strengths.

Table 1. SZ catalysts tested in glucose hydrolysis.

Catalyst	Preparation Method	Crystalline Phase	Effective (Nominal) Sulphate *w*/*w*%
S2Z_W1	WI on t-ZrO_2	t- + m-ZrO_2 (Vm = 0.04)	0.67
S1Z_5	IWI on xerogel	t-ZrO_2 + amorphous	2.80 (5)
S2Z_8	IWI on t-ZrO_2	t-ZrO_2 [1]	6.46 (8)
SZ_p	precipitation route	t-ZrO_2 [1]	5.25 (8)

[1] PXRD data in Figure S5.

2.3.1. FTIR Study of Surface Properties of SZ Catalysts

It has been proposed that the amount of surface sulphates do not give per se all information concerning the properties of a SZ-based catalyst, being the nature of the sulphates more important than just its presence [44]. Sulphate groups formed at the surface of metal oxides are known to possess a highly heterogeneous nature, and they are characterised by complex spectral features. FTIR spectral features of surface sulphates are affected by the overall degree of surface hydration. On the highly hydrated surface, as those observed in the ATR spectra (in Figure S3), the formation of several broad bands in the 1200–900 cm^{-1} range have been related to sulphates mainly in an ionic configuration, resembling that of inorganic (bidentate) sulphate complexes [45,46]. On medium-highly dehydrated surfaces, sulphates tend to acquire a more covalent configuration that allows them to better discriminate their nature.

In the spectra of activated samples, reported in Figure 3a, at high wavenumbers, we can observe signals due to the stretching of the terminal and bridged OH groups [46]. For SZ_p, these signals are present, respectively, as a weak band centred at 3745 cm^{-1} and a strong band at 3645 cm^{-1}, similar to data reported in the literature for sulphated-promoted t-ZrO_2 [7,47]. For samples obtained by means of MW-assisted synthesis, we can observe spectral components due to (i) terminal OH groups (at 3765 cm^{-1}), (ii) a broad band at lower wavenumbers related to the stretching modes of bridged OH (shoulder around 3650 cm^{-1}) and (iii) OH groups involved in H-bonding (broader envelope). The presence of these signals suggests that only a low-medium degree of dehydration is achieved on samples obtained by MW-assisted synthesis. At the surface of these materials, other spectral components are evident below 1700 cm^{-1} (see Figure 3b). On the basis of their spectral features [48], there might be present some residual carbonate species (not removed after thermal activation). In the case of S2Z_WI (blue curves in Figure 3b), a broad band at ~1560 cm^{-1} and a tiny signal at 1450 cm^{-1} are quite evident and may be ascribed, respectively, to bi- and mono-dentate carbonate species [48]. No similar signals are present in the SZ_p spectrum, suggesting that carbonate species are formed on the surface of the material during the MW-assisted calcination, which is carried out in a static atmosphere and the presence of incandescent graphite.

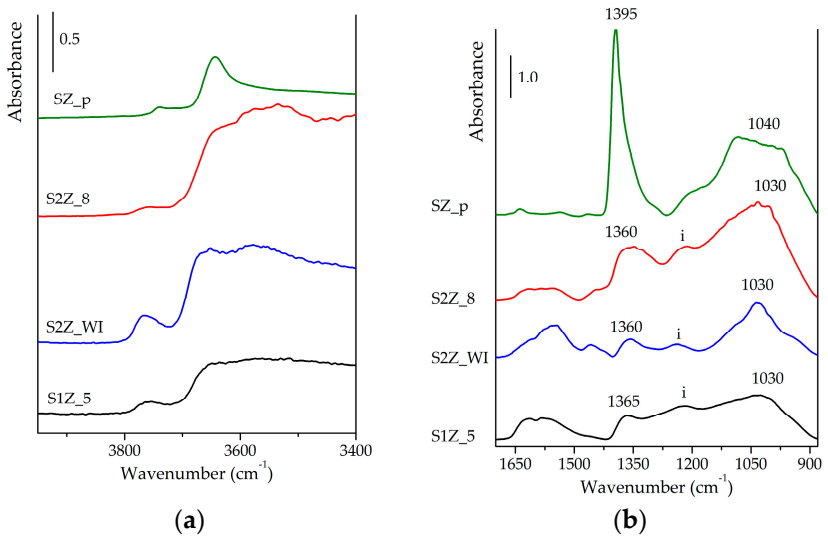

Figure 3. FTIR spectra of SZ_p (in green), S2Z_8 (in red), S2Z_WI (in blue) and S1Z_5 (in black), recorded after activation at 300 °C in the OH spectral region (**a**) and in the 1700-880 cm^{-1} spectral region (**b**).

In the 1400–1000 cm^{-1} spectral range, it is possible to observe signals of sulphate species, see Figure 3b. The spectrum of activated SZ_p shows (i) an intense signal at 1395 cm^{-1} related to the S=O asymmetric stretching mode, (ii) a broad band at ca 1040 cm^{-1} due to the S–O stretching and (iii) a weak peak at 1180 cm^{-1} ascribable to the (O=S=O) symmetric mode. The increase of the spectral separation between high and low-frequency modes is ascribable to a high covalent character achieved by sulphates [5,44,46]. S2Z_8 and S2Z_WI exhibit comparable behaviour after activation. The band of the S=O mode at 1360 cm^{-1} is broad and relatively weak, and the broad band of the S–O mode is centred at ~1030 cm^{-1}: both are attributable to sulphate species with a covalent character. There is also a broad and complex band centred at 1230 cm^{-1} (indicated as **i** in Figure 3b), suggesting that part of surface sulphates still possess a mainly ionic character, and S2Z_WI seems to present a major fraction of surface sulphates with covalent configuration. The spectrum of activated S1Z_5 exhibits a partially structured broad band in the 1400–900 cm^{-1} range. The presence of at least a fraction of covalent surface sulphates is supported by the spectral pair at 1365 and 1030 cm^{-1}, but the relatively high intensity of the band at 1220 cm^{-1}

could suggest that a large part of sulphates still retain a more ionic configuration. On the basis of these spectral features, it can be inferred that the nature of surface sulphate is strongly affected by both preparation and calcination methods, as already suggested in the literature [3,5]. If compared to SZ calcined in a conventional way, samples calcined by the MW-assisted procedure present sulphates with a less covalent character. Comparing the impregnation methods, the covalent character of surface sulphates is more pronounced in the sample prepared by WI (S2Z_WI) that possesses a low amount of sulphate groups. Samples impregnated with a larger amount of sulphating agent by the IWI procedure seem to present a major fraction of sulphates with ionic configuration.

Both presence and strength of L and B acid sites have been investigated by FTIR spectroscopy of adsorbed probe molecules: CO [48–50] and 2,6-DMP [51–54].

For plain and sulphated t-ZrO_2, the RT adsorption of CO (reported in Figure 4a) has been shown to yield a strong signal in the 2200–2180 cm^{-1} spectral range, related to CO interacting with coordinatively unsaturated surface (cus) Zr^{4+} cations located in defective crystallographic positions: CO frequency increases upon sulphation indicating an increase of the L acidity of cus cations [48,55]. In the case of plain t-ZrO_2 (Z1), CO adsorption gives rise to a strong signal at 2181 cm^{-1} and to a shoulder at 2155 cm^{-1}, well recognisable at maximum pressure (100 torr). The former signal is ascribable to CO adsorbed on the most acid L sites, i.e., cationic sites located on defective crystallographic configuration, and the latter has been assigned to CO uptake onto more ordered sites, i.e., cus cationic sites located on extended patches of regular crystal planes [48]. Upon CO adsorption on the SZ_p sample, a strong and sharp signal is observed at 2200 cm^{-1}, which decreases in intensity with decreasing CO coverage, as shown in Figure 4b, suggesting the presence of strong L sites. In the SZ samples obtained by the MW-assisted method, the related signal can be observed at lower wavenumbers (as shown in Figures 4c and S6), and so L strength is supposed to decrease as follow: SZ_p > S2Z_8 > S1Z_5 > S2Z_WI. The intensity of the signal of SZ samples is comparable to that of Z1 one, suggesting that sulphation reduces only partially the number of L-acid sites and increases only to a very limited extent their acid strength. For all MW-synthesised samples, it is possible to observe a shoulder at 2155 cm^{-1}, probably related to CO absorption on regular planes. We may suppose that this feature could be related to the MW-assisted calcination step, which seems to generate heterogeneous surface sulphates that occupy both defective and regular sites, while on 'model' systems, only the defective sites are set free and may interact with CO molecules.

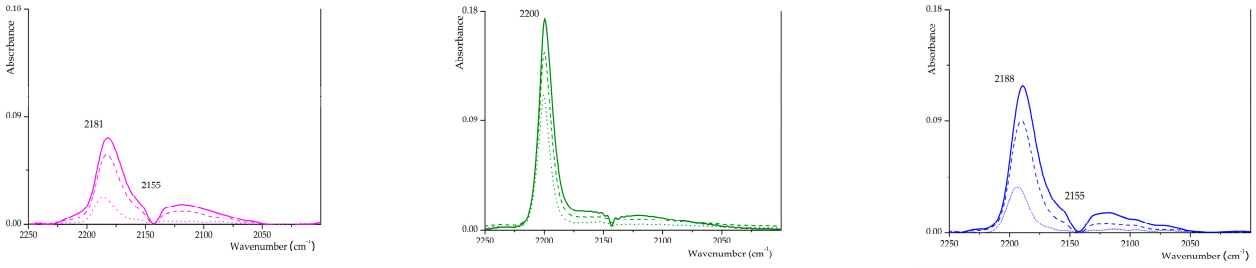

(**a**) (**b**) (**c**)

Figure 4. Differential FTIR spectra of CO adsorbed on (**a**) Z1, (**b**) SZ_p and (**c**) S2Z_WI. The solid line for 100 torrs, the dashed line for 50 torrs, and the dotted line for 5 torr.

2,6-DMP uptake can reveal the presence of acidic sites that differ either in nature (i.e., L or B) and/or in acidic strength. 2,6-DMP adsorption on SZ_p (in Figure 5a) gives rise to spectra similar to those reported for similar tetragonal SZ [51]. At the maximum pressure (~4 torr), the strongest signals are represented by the two bands at 1594 and 1580 cm^{-1} (ascribable to H-bonded and physisorbed 2,6-DMP molecules, respectively), with a shoulder at 1604 cm^{-1}, due to L-coordinated 2,6-DMP, and by a broad envelope above 1620 cm^{-1}, due to 2,6-$DMPH^+$ strongly held to the surface, indicating the presence of medium-strength B acid sites. Upon outgassing, the overall intensity of the envelope at lower wavenumbers

decreases drastically, as expected for the elimination of physisorbed/weakly held species, but bands at 1580, 1594, and 1608 cm^{-1} are still observable, suggesting the presence of strong L acid centres. The spectral features of 2,6-$DMPH^+$ species remain strong, with only a partial modification in intensity and profile as well. For S2Z_8 (in Figure 5b), we can notice that at the maximum pressure, the strongest band is related to 2,6-$DMPH^+$ modes, whose spectral profile remains virtually unchanged after outgassing. Signals related to the strongest L acid sites, which retain 2,6-DMP at low pressure, are observable at 1578, 1594 and 1604 cm^{-1}, similar to those observed in a 'model' system. On the contrary, both S2Z_WI and S1Z_5 exhibit a different behaviour: these two samples present the two bands related to 2,6-$DMPH^+$ modes at 1648 and 1629 cm^{-1}, ascribable to B acidity, and below 1620 cm^{-1}, a resistant fraction of physisorbed and/or H-bonded 2,6-DMP is evident, giving rise to a multiple band still intense after evacuation. Curve fitting (by means of the facility present in the OMNIC software) of this unresolved band (in the inset of Figure 5c,d) suggests that it is composed of 3 distinct components located at ~1582, 1596 and 1604 cm^{-1}, respectively—analogous to those observed in SZ_p and S2Z_8. The shape and position of these spectral components are more similar to that reported for t-ZrO_2 [51] with respect to other analysed SZ materials. This suggests that for S1Z_5 and S2Z_WI sulphation effects, to a limited extent, the strength of the L acidity, even if the B acid sites are present on the surface. On the basis of the spectral features that were previously described, the proposed scale of the strength of L acidity is analogous to that suggested by CO absorption, and the same trend is also suggested for B acidity (SZ_p > S2Z_8 > S2Z_WI > S1Z_5).

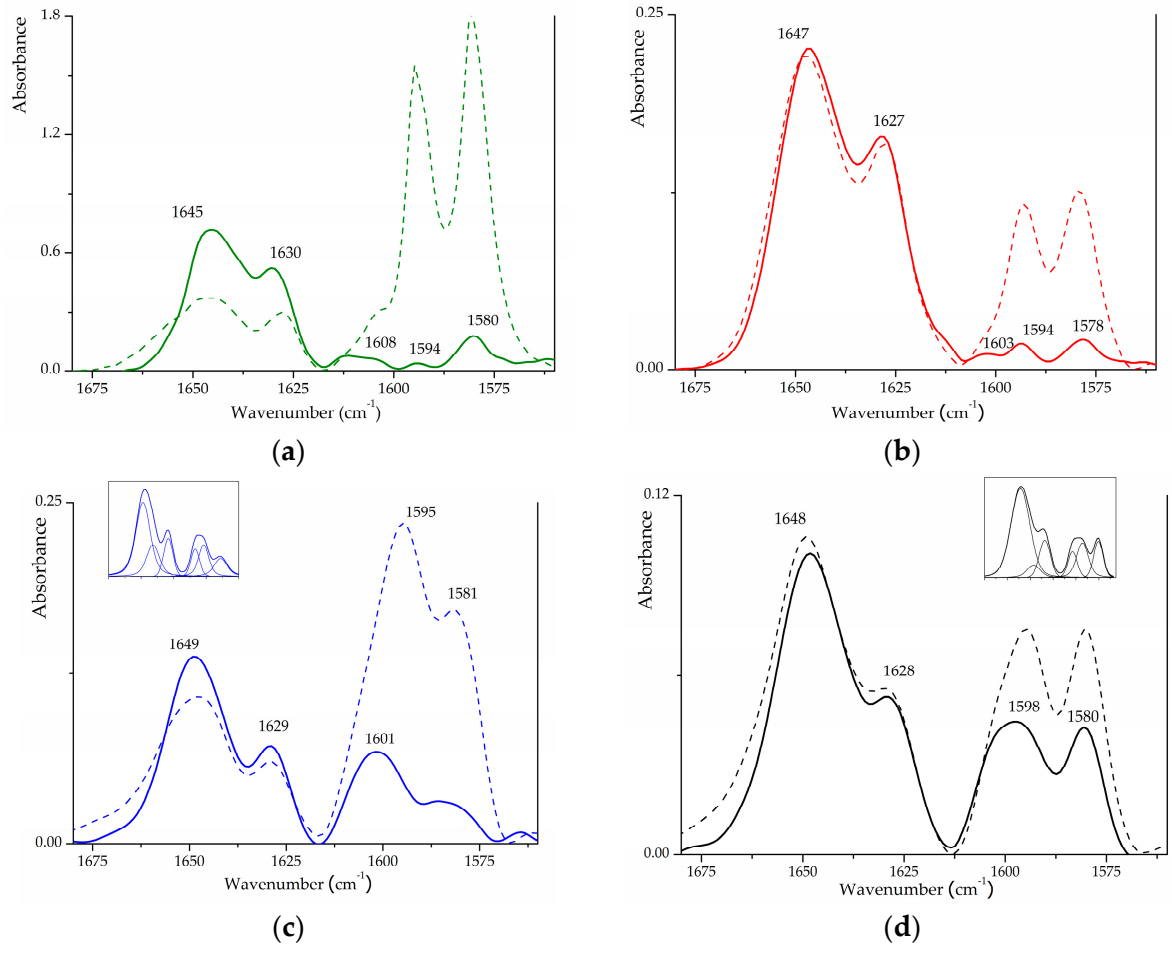

Figure 5. Differential FTIR spectra of 2,6-DMP adsorbed on (**a**) SZ_p, (**b**) S2Z_8, (**c**) S2Z_WI, (**d**) S1Z_5. Dash line under maximum pressure, solid line after evacuation for 15 min. In the insets, deconvolution of the observed band.

2.3.2. Catalytic Tests in Glucose Hydrolysis

Acid hydrolysis of glucose was carried out at 180 °C in a solution with a low concentration of substrate (0.027 M) to minimise the side reactions of the products, as suggested by similar studies [15,17]. Experimentally, it has been noted that glucose-to-fructose isomerisation is favoured by L acid catalyst at 90~120 °C, while the fructose-to-HMF dehydration is promoted by both L and B acid catalysts at higher reaction temperatures (120–200 °C) [16]. Humins are unavoidable by-products that can significantly affect yield and cause catalyst deactivation and adsorbed intermediates and substrates. The formation of humins is suggested to be strongly affected by the initial substrate concentration, being produced in a second-order reaction [56].

Results relative to catalytic tests are reported and compared in Table 2. Different reaction times (from 1 to 5 h) were tested for S2Z_WI: yield of 5-HMF increases, extending reaction time, and a good yield of 5-HMF (~35%) can be obtained, with good selectivity. Using S2Z_8, glucose conversion is significantly improved with a long reaction time, enhancing 5-HMF production (~15%) and promoting the formation of small amounts of LA (~3%). On the contrary, S1Z_5 exhibits poor selectivity, and the formation of a small amount of 5-HMF (6.5%) was observed even for a long reaction time. Glucose conversion is high, but the carbon balance is very low, suggesting that glucose might proceed towards possible derivatives by degradation/condensation processes. The 'model' catalyst SZ_p promotes the formation of 5-HMF (17%) and LA (3.4%) after 3 h, but the low carbon balance suggests the formation of humins as a by-product.

Table 2. Results of catalytic tests for SZ samples and SZ in the literature.

Catalyst	Reaction Condition	Conversion %	C Balance %	Product Yield (Selectivity) %		
				5-HMF	LA	HCOOH
S2Z_W1	180 °C, 1 h	60.0	47.3	26.1 (43.4)	0.17 (0.28)	1.02 (1.70)
S2Z_W1	180 °C, 3 h	76.0	47.7	28.0 (36.9)	0.17 (0.22)	6.74 (8.87)
SZ_p	180 °C, 3 h	88.9	28.9	17.0 (19.1)	3.43 (3.86)	4.09 (4.60)
S2Z_8	180 °C, 3 h	59.0	16.6	10.1 (17.1)	0.12 (0.21)	0.00 (0.00)
S2Z_WI	180 °C, 5 h	78.0	49.3	34.9 (44.8)	0.18 (0.23)	1.71 (2.19)
S2Z_8	180 °C, 5 h	91.4	24.0	14.6 (15.9)	3.29 (3.60)	2.67 (2.92)
S1Z_5	180 °C, 5 h	91.3	7.7	6.4 (7.1)	0.12 (0.13)	0.24 (0.26)
SO_4^{2-}/ZrO_2 [17]	120 °C, 6 h	23.3	99	(3.7)	–	–
SO_4^{2-}/ZrO_2 [57]	130 °C, 4 h [1]	95.2	–	(19.2)	–	–
SO_4^{2-}/ZrO_2 [58]	160 °C, 2 h [2]	52	–	42	19	21

[1] DMSO; [2] NaCl-THF/H_2O.

According to the surface properties of the previously described catalysts, we can raise some consideration on their both activity and selectivity. SZ_p possesses surface sulphate groups with a high covalent character that generates strong L and B sites. The latter is suggested to promote glucose isomerisation, and both act on the following hydration/dehydration reactions. The presence of a strong B site promotes rehydration to 5-HMF in LA but seem also to favour condensation reaction(s), thus affecting selectivity. Catalyst S2Z_8 presents medium-strong L and B acid sites, which promote the formation of both 5-HMF and LA, exhibiting long reaction times and giving low yields. Also, in this case, the formation of condensation products seems to be favoured. The catalyst that is supposed to possess a weak B acid site, such as S2Z_WI, on the contrary, promotes the formation of 5-HMF with good yield but not the further hydrolysis to LA, even increasing reaction time. This suggests that the formation of LA requires the presence of a stronger B acid site. Fructose yield was found to be maximal when the reaction is stopped after 1 h, suggesting that the reaction passes through glucose isomerisation to produce 5-HMF, but longer reaction times are required to improve glucose conversion. S1Z_5 shows poor catalytic activity, even if L and B sites have been recognised to be present on its surface and the amount of sulphates is higher with respect to S2Z_WI.

3. Discussion

We proposed an MW-assisted sol-gel procedure to obtain ZrO_2 that involves two steps of a few minutes, both assisted by MW heating. In the former, the gel is dried (MW-assisted drying), and in the latter, the obtained xerogel is calcined using a susceptor that rapidly reaches a high temperature (MW-assisted calcination). Homogeneous ZrO_2 NPs exhibiting pure tetragonal phase have been obtained, as indicated by both vibrational and structural characterisations. Only a few similar studies have been reported in the literature so far, and MW irradiation was applied in the sol-gel synthesis of ZrO_2 in different steps: gel formation [27,29], drying [28] and calcination [29]. In all cases, the formation of the tetragonal phase, as in our procedure, is favoured, suggesting that MW heating promotes the formation of t-ZrO_2. It is interesting to notice that if MW irradiation is applied in gel formation or drying, it is then necessary to calcine the powder (in a traditional way) to obtain a crystalline product. Our results indicate that MW-assisted calcination can be efficiently applied to different zirconium oxy-hydroxide intermediates (i.e., obtained from $ZrOCl_2$ and/or $Zr(OCH_2CH_2CH_3)_4$). MW hybrid heating methods, which employ a susceptor to transfer heat to the sample, have been applied previously in materials production [31], but to the best of our knowledge, never to carry out calcination on amorphous materials. This innovative approach allows for extremely reduced calcination time and energy consumption compared to traditional thermal treatments.

We applied the proposed procedure to the synthesis of SZ, a well-known solid acid catalyst. After impregnation with the proper sulphating agent (by WI or IWI) on xerogel or the already formed t-ZrO_2, dried powders were thermally treated by MW-assisted calcination. It is generally reported that sulphation on zirconia intermediates leads to a stabilisation of the tetragonal phase [3,37], while in our procedure, sulphation seems to inhibit crystallisation of amorphous intermediate and to promote a modest growth of monoclinic fraction on impregnated t-ZrO_2 NPs. Depending on the impregnation step, SZ possesses sulphate species with different characteristics: covalent on samples obtained by impregnation on t-ZrO_2 and a more ionic nature when the impregnation is carried out on the xerogel. Both nature and strength of acidic surface sites have been investigated using CO and 2,6-DMP as probe molecules. Results indicate that both L and B acid sites are present, but their relative strength is influenced by the impregnation method and the impregnation step as well.

So, we decided to test SZ as a catalyst in glucose hydrolysis, a reaction that proceeds in consecutive steps catalysed by L and/or B sites. We tested four SZ catalysts with L and B sites at increasing strengths:

(i) S1Z_5 (by IWI xerogel) partially amorphous, showing surface sulphates with a less pronounced covalent character and presenting weak L and B acid sites;
(ii) S2Z_WI (by WI on t-ZrO_2) having surface sulphates with a covalent character and presenting weak L and B sites;
(iii) S2Z_8 (by WI on t-ZrO_2) that has surface sulphate species with covalent character and present L and B acid sites of medium strength;
(iv) a 'model' SZ (obtained from standard precipitation route) presenting strong L and B acid sites.

S1Z_5 shows poor catalytic activity, even if weak L and B sites have been recognised on its surface. The presence of a stable L or B acidity on SZ is a necessary but not sufficient condition to observe the catalytic activity. Morterra et al. [51] have already evidenced this behaviour in SZ catalysts employed in the mild temperature isomerisation of *n*-butane, a standard reference reaction to test the catalytic activity of SZ-based materials. The presence of L and B sites with medium or strong strength promotes further 5-HMF rehydration to formic acid (FA) and LA, but also condensation reactions. The detrimental effect in selectivity of B acid sites in glucose hydrolysis has been recently proposed by Li et al. [13].

The catalyst that is supposed to possess weak L and B acid sites, such as S2Z_WI, shows better selectivity toward 5-HMF, confirming the fundamental role of weak acid sites in promoting 5-HMF formation in water media, as also recently suggested in the

literature [12,13]. For this catalyst, we observed a better selectivity to 5-HMF with respect to the 'model' system (SZ_p) and to studies reported in the literature (see Table 2). In particular, we noted a higher glucose conversion with respect to the results reported by Osatiashtiani et al. [17], which could be related to both higher reaction temperatures and different crystalline phases of the SZ catalyst. Other studies were conducted in DMSO [57] and biphasic systems [58], in which further rehydration reaction of 5-HMF to LA and the formation of large molecular weight humins is limited, but yields are still comparable. These results suggest that selectivity in glucose hydrolysis in water is more related to the strength rather than to the number of acid sites.

In conclusion, our results suggest that MW-assisted synthesis could be employed to obtain a well-known catalyst with a less energy-consuming procedure. One of the obtained SZ samples has shown good catalytic activity in 5-HMF production in water due to the co-presence of weak L and B acid sites on its surface.

4. Materials and Methods

All chemicals of analytical grade were purchased by Sigma-Aldrich Products (St. Louis, MO, USA). As the MW heating system, an adapted household multimodal MW oven (SAMSUNG C109STF, working at 2.45 GHz) was used. The multimodal MW oven can operate at different power levels: 180 W, 300 W, 450 W, 600 W, and 900 W. It works in continuous mode at the higher power level and in pulsed mode at lower levels, with an on-off cycle of irradiation (20 s on, 10 s off).

4.1. Synthesis

The general procedure for the preparation of ZrO_2 nanoparticles involved three steps. At first, the gel was formed by adding water dropwise in a solution containing 5 mL of $Zr(OCH_2CH_2CH_3)_4$ (70 wt%, in 1-propanol), 7 mL of ethanol and the appropriate amount of the acid hydrolysis catalyst to obtain a final pH~2. In the second step (named MW-assisted drying), the gel obtained was dried in an MW oven to remove the solvent rapidly by evaporation (2 cycles of 90 s at 600 W). The obtained xerogel was washed with ethanol and dried in air. In order to obtain a crystalline product, a further thermal treatment at high temperature was carried out in an MW oven using graphite as an external susceptor (~10 g per 1.6 g of xerogel; synthetic powder, <20 μm). To promote homogeneous heating of the sample, a two crucibles set-up was employed: the smaller crucible containing the sample is placed in a larger crucible filled with the graphite powder (see Figure S7) [31]. The thermal treatment is named MW-assisted calcination and requires two cycles of 90 s at 600 W. Starting from 5 mL of zirconium precursor, about 1.2 g of ZrO_2 was obtained.

Z1 was obtained using nitric acid as a catalyst to promote hydrolysis. Z2 was prepared according to a general procedure, but the xerogel was calcinated in a muffle at 450 °C for 1 h (dT/dt = 5 °C/min). Z3 was prepared by a controlled co-precipitation from aqueous solutions of $ZrOCl_2 \cdot 8H_2O$, carried out at room temperature and at pH = 8.5 adding, when necessary, NH_4OH 5.0 M. The precipitate was aged in the mother liquor for 20 h at 90 °C, filtrated and washed from chloride ions. MW-assisted calcination was carried out on dry powdery materials.

Sulphate species were added using $(NH_4)_2SO_4$ by either wetness impregnation (WI) or by incipient wetness impregnation (IWI) on xerogels prior to calcination or on ZrO_2. MW-assisted calcination was carried out on dried impregnated samples (2 cycles of 90 s at 600 W for impregnated xerogel and two cycles of 90 s at 450 W for impregnated zirconia). Samples were designated as SxZ_y where x stands for addition step (1 = impregnated on xerogel, 2 = impregnated on ZrO_2) and y stands for sulphates nominal content (as wt%). For WI, a $(NH_4)_2SO_4$ solution 0.5 M was employed.

Our materials were compared to a 'model' system: sulphated zirconia prepared by a standard precipitation route (SZ_p) synthesised according to the precipitation method described above, but the dry powder obtained after washing was impregnated with 8 wt% of

sulphates (using ($(NH_4)_2SO_4$) and then calcinated in a furnace at 555 °C (dT/dt = 10 °C/min) for 180 min under airflow (30 mL/min).

4.2. Characterizations

The structure and crystallinity of the samples were investigated by X-ray diffraction powder (PXRD) using an X'Pert powder diffractometer operating in a Bragg–Brentano geometry, equipped with a graphite crystal monochromator and using Cu($K_{\alpha 1}$) radiation (1.5406 Å) and step size of 0.02°. Monoclinic volume was calculated using the Toraya equation [59]. The fitting procedure of the experimental diffractograms was made in the 27–33° range using Lorentzian curves to determine the integrated intensity of individual signals.

Raman spectra were recorded on pure samples using a Bruker Vertex 70 spectrometer, equipped with the RAMII accessory and Ge detector, by exciting samples with Nd:YAG laser source (1064 nm), with a resolution of 4 cm^{-1}. Monoclinic volume was calculated using the equation proposed by Tabares et al. [60]. The integrated intensity of individual peaks was obtained with a fitting procedure using a Lorentzian curve on a linear background in the 125–205 cm^{-1} spectral range. ATR-FTIR spectra were obtained with the same instrument with Harrick MVP2 ATR cell and DTGS detector (64 scans, 2 cm^{-1} resolution).

FTIR spectra were recorded using a Bruker IFS28 spectrometer equipped with an MCT detector at 4 cm^{-1} resolution. The solid samples, in the form of self-supported pellets (≈10 mg/cm^2), were inserted in a conventional quartz vacuum cell equipped with KBr windows connected to a glass vacuum line (residual pressure < 10^{-5} Torr) that allows for performance in situ adsorption/desorption runs. Samples were activated at 300 °C and treated under an oxidising environment. Adsorption/desorption tests of 2,6-dimethylpyridine (2,6-DMP) and CO were carried out at ambient temperature. First, 100 torrs of CO were allowed on the sample and then totally evacuated, recording spectra at decreasing pressure. Then a relatively large amount of 2,6-DMP (~4 Torr) was allowed on the samples and left in contact for 2 min to reach a complete monolayer formation, and then the 2,6-DMP excess was evacuated for increasing times in the 1–15 min range to put into evidence only the more strongly held fraction. Differential spectra were obtained by subtracting the spectra of activated catalysts from the spectra obtained after adsorption/desorption runs.

High-resolution transmission electron microscopy (HR-TEM) images of the samples were acquired with a JEOL JEM 3010 UHR operating at 300 kV, equipped with a LaB_6 filament and an Oxford Inca spectrometer for energy-dispersive X-ray spectroscopy (EDS) determinations. All powders were 'dry' dispersed on Cu grids coated with lacey carbon film.

The amount of sulphates was determined by ion chromatography following a well-established procedure reported in the literature [44].

4.3. Catalytic Tests

Different sulphated zirconia samples were employed as catalysts in glucose hydrolysis (SZ_WI, SZ_prec, S1Z_5, S2Z_8). The reaction was carried out in a batch stainless steel autoclave with mechanical stirring and an electric heater. Before the reaction, 500 mg substrate, 100 mL of water and an appropriate amount of catalyst (from 200 to 500 mg) were added to the reactor and then heated to 180 °C under a 10-bar pressure of N_2. The initial time of the reaction was taken once the reaction temperature was reached (around 1.5 h). The reaction was carried out for 1–5 h at 1000 rpm. After this time, the mixture was cooled down to room temperature and separated by filtration. The reaction mixture was analysed by HPLC (Agilent Technology 1260 Infinity II) equipped with an Aminex HPX-87H column kept at 50 °C. The mobile phase was 5 mM H_2SO_4 with a flow rate of 0.6 mL/min. UV-Vis detector (at 195 nm) was used for the identification of the analytes and their quantitative determination. Reactivity parameters were calculated based on moles

of carbon as follows, where *i* represents a general product of the reaction and G stands for glucose:

$$\text{G conversion (\%)} = \{[(\text{mol}_\text{G} \text{ in}) - (\text{mol}_\text{G} \text{ out})]/(\text{mol}_\text{G} \text{ in})\} \times 100 \quad (1)$$

$$\text{C balance (\%)} = \text{C out/C in} = [(\text{mol of C in product})/(\text{mol of C in G converted})] \times 100 \quad (2)$$

$$\text{Yield } i \text{ (\%)} = [(\text{mol } i \text{ out})/(\text{mol G in})] \times 100 \quad (3)$$

$$\text{Selectivity } i \text{ (\%)} = [(\text{Yield } i)/(\text{Glucose conversion})] \times 100 \quad (4)$$

Supplementary Materials: The following supporting information can be downloaded at: https://www.mdpi.com/article/10.3390/catal13071094/s1, Figure S1: Experimental PXRD of Z1, Z2, Z3 and of the product obtained using acetic acid as hydrolysis catalyst compared to reference for t-ZrO_2; Figure S2: ATR spectra of products obtained after MW-drying (dotted lines) and MW-calcination using sulfuric, nitric, and acetic acid as hydrolysis catalysts (in red, black, and blue, respectively); Figure S3: Raman spectra of S1Z and S2Z, impregnated by IWI with sulphates at increasing wt%; Figure S4: ATR spectra of S1Z_WI, S2Z_WI, and S1Z and S2Z impregnated by IWI with sulphates at increasing wt%; Figure S5: A Raman spectrum and powder diffractogram of catalysts SZ_p and S2Z_8; Figure S6: Differential FTIR spectra of CO adsorbed on S2Z_8 and S1Z_5; Figure S7: Schematic representation of the two crucibles set-up employed during MW-assisted calcination. Temperature measurements during MW-assisted calcination description. References [21,31,61] are cited in the Supplementary Materials.

Author Contributions: Conceptualization, A.G. and G.C.; methodology, A.G., G.C., E.G. and M.S.; validation, A.G., G.C. and L.O.; formal analysis, A.G. and C.P.; investigation, A.G., C.P. and E.G., resources, G.C.; data curation, A.G., G.C., L.O. and M.S.; writing—original draft preparation, A.G. and G.C.; writing—review and editing, A.G., G.C., M.S., E.G. and L.O.; supervision, G.C. and M.S. All authors have read and agreed to the published version of the manuscript.

Funding: This research received no external funding.

Data Availability Statement: Not applicable.

Conflicts of Interest: The authors declare no conflict of interest.

References

1. Hino, M.; Arata, K. Synthesis of Solid Superacid Catalyst with Acid Strength of $H_0 \leq -16.04$. *J. Chem. Soc. Chem. Commun.* **1980**, *18*, 851–852. [CrossRef]
2. Song, X.; Sayari, A. Sulfated Zirconia-Based Strong Solid-Acid Catalysts: Recent Progress. *Catal. Rev.* **1996**, *38*, 329–412. [CrossRef]
3. Yan, G.X.; Wang, A.; Wachs, I.E.; Baltrusaitis, J. Critical Review on the Active Site Structure of Sulfated Zirconia Catalysts and Prospects in Fuel Production. *Appl. Catal. Gen.* **2019**, *572*, 210–225. [CrossRef]
4. Comelli, R.A.; Vera, C.R.; Parera, J.M. Influence of ZrO_2 Crystalline Structure and Sulfate Ion Concentration on the Catalytic Activity of $SO_4{}^{-2}$–ZrO^2. *J. Catal.* **1995**, *151*, 96–101. [CrossRef]
5. Morterra, C.; Cerrato, G.; Signoretto, M. On the Role of the Calcination Step in the Preparation of Active (Superacid) Sulfated Zirconia Catalysts. *Catal. Lett.* **1996**, *41*, 101–109. [CrossRef]
6. Stichert, W.; Schüth, F. Synthesis of Catalytically Active High Surface Area Monoclinic Sulfated Zirconia. *J. Catal.* **1998**, *174*, 242–245. [CrossRef]
7. Morterra, C.; Cerrato, G.; Meligrana, G.; Signoretto, M.; Pinna, F.; Strukul, G. Catalytic Activity and Some Related Spectral Features of Yttria-Stabilised Cubic Sulfated Zirconia. *Catal. Lett.* **2001**, *73*, 113–119. [CrossRef]
8. Kumari, N.; Sareen, S.; Verma, M.; Sharma, S.; Sharma, A.; Sohal, H.S.; Mehta, S.K.; Park, J.; Mutreja, V. Zirconia-Based Nanomaterials: Recent Developments in Synthesis and Applications. *Nanoscale Adv.* **2022**, *4*, 4210–4236. [CrossRef]
9. Joo, J.B.; Vu, A.; Zhang, Q.; Dahl, M.; Gu, M.; Zaera, F.; Yin, Y. A Sulfated ZrO_2 Hollow Nanostructure as an Acid Catalyst in the Dehydration of Fructose to 5-Hydroxymethylfurfural. *ChemSusChem* **2013**, *6*, 2001–2008. [CrossRef]
10. Zhang, W.; Wang, Z.; Huang, J.; Jiang, Y. Zirconia-Based Solid Acid Catalysts for Biomass Conversion. *Energy Fuels* **2021**, *35*, 9209–9227. [CrossRef]
11. Bozell, J.J.; Petersen, G.R. Technology Development for the Production of Biobased Products from Biorefinery Carbohydrates—The US Department of Energy's "Top 10" Revisited. *Green Chem.* **2010**, *12*, 539. [CrossRef]

12. Zhu, L.; Fu, X.; Hu, Y.; Hu, C. Controlling the Reaction Networks for Efficient Conversion of Glucose into 5-Hydroxymethylfurfural. *ChemSusChem* **2020**, *13*, 4812–4832. [CrossRef] [PubMed]
13. Li, X.; Peng, K.; Liu, X.; Xia, Q.; Wang, Y. Comprehensive Understanding of the Role of Brønsted and Lewis Acid Sites in Glucose Conversion into 5-Hydromethylfurfural. *ChemCatChem* **2017**, *9*, 2739–2746. [CrossRef]
14. Agarwal, B.; Kailasam, K.; Sangwan, R.S.; Elumalai, S. Traversing the History of Solid Catalysts for Heterogeneous Synthesis of 5-Hydroxymethylfurfural from Carbohydrate Sugars: A Review. *Renew. Sustain. Energy Rev.* **2018**, *82*, 2408–2425. [CrossRef]
15. Kang, S.; Fu, J.; Zhang, G. From Lignocellulosic Biomass to Levulinic Acid: A Review on Acid-Catalyzed Hydrolysis. *Renew. Sustain. Energy Rev.* **2018**, *94*, 340–362. [CrossRef]
16. Yang, G.; Pidko, E.A.; Hensen, E.J.M. Mechanism of Brønsted Acid-Catalyzed Conversion of Carbohydrates. *J. Catal.* **2012**, *295*, 122–132. [CrossRef]
17. Osatiashtiani, A.; Lee, A.F.; Brown, D.R.; Melero, J.A.; Morales, G.; Wilson, K. Bifunctional SO_4/ZrO_2 Catalysts for 5-Hydroxymethylfufural (5-HMF) Production from Glucose. *Catal. Sci. Technol.* **2014**, *4*, 333–342. [CrossRef]
18. Kitchen, H.J.; Vallance, S.R.; Kennedy, J.L.; Tapia-Ruiz, N.; Carassiti, L.; Harrison, A.; Whittaker, A.G.; Drysdale, T.D.; Kingman, S.W.; Gregory, D.H. Modern Microwave Methods in Solid-State Inorganic Materials Chemistry: From Fundamentals to Manufacturing. *Chem. Rev.* **2014**, *114*, 1170–1206. [CrossRef]
19. Tompsett, G.A.; Conner, W.C.; Yngvesson, K.S. Microwave Synthesis of Nanoporous Materials. *ChemPhysChem* **2006**, *7*, 296–319. [CrossRef]
20. Zhu, Y.-J.; Chen, F. Microwave-Assisted Preparation of Inorganic Nanostructures in Liquid Phase. *Chem. Rev.* **2014**, *114*, 6462–6555. [CrossRef]
21. Mirzaei, A.; Neri, G. Microwave-Assisted Synthesis of Metal Oxide Nanostructures for Gas Sensing Application: A Review. *Sens. Actuators B Chem.* **2016**, *237*, 749–775. [CrossRef]
22. Manjunatha, S.; Dharmaprakash, M.S. Microwave Assisted Synthesis of Cubic Zirconia Nanoparticles and Study of Optical and Photoluminescence Properties. *J. Lumin.* **2016**, *180*, 20–24. [CrossRef]
23. Hembram, K.P.S.S.; Mohan Rao, G. Microwave Synthesis of Zirconia Nanoparticles. *J. Nanosci. Nanotechnol.* **2008**, *8*, 4159–4162. [CrossRef] [PubMed]
24. Bondioli, F.; Ferrari, A.M.; Leonelli, C.; Siligardi, C.; Pellacani, G.C. Microwave-Hydrothermal Synthesis of Nanocrystalline Zirconia Powders. *J. Am. Ceram. Soc.* **2001**, *84*, 2728–2730. [CrossRef]
25. Liang, J.; Deng, Z.; Jiang, X.; Li, F.; Li, Y. Photoluminescence of Tetragonal ZrO_2 Nanoparticles Synthesized by Microwave Irradiation. *Inorg. Chem.* **2002**, *41*, 3602–3604. [CrossRef] [PubMed]
26. Batool, T.; Bukhari, B.S.; Riaz, S.; Batoo, K.M.; Raslan, E.H.; Hadi, M.; Naseem, S. Microwave Assisted Sol-Gel Synthesis of Bioactive Zirconia Nanoparticles—Correlation of Strength and Structure. *J. Mech. Behav. Biomed. Mater.* **2020**, *112*, 104012. [CrossRef]
27. Fetter, G.; Bosch, P.; Pez, T.L. ZrO_2 and Cu/ZrO_2 Sol-Gel Synthesis in Presence of Microwave Irradiation. *J. Sol-Gel Sci. Technol.* **2002**, *23*, 199–203. [CrossRef]
28. Dwivedi, R.; Maurya, A.; Verma, A.; Prasad, R.; Bartwal, K.S. Microwave Assisted Sol–Gel Synthesis of Tetragonal Zirconia Nanoparticles. *J. Alloys Compd.* **2011**, *509*, 6848–6851. [CrossRef]
29. Silva Junior, E.; Antonio, S.G.; Longo, E. Synthesis and Structural Evolution of Partially and Fully Stabilized ZrO_2 from a Versatile Method Aided by Microwave Power. *Ceram. Int.* **2018**, *44*, 3517–3522. [CrossRef]
30. Mishra, R.R.; Sharma, A.K. Microwave–Material Interaction Phenomena: Heating Mechanisms, Challenges and Opportunities in Material Processing. *Compos. Part Appl. Sci. Manuf.* **2016**, *81*, 78–97. [CrossRef]
31. Bhattacharya, M.; Basak, T. A Review on the Susceptor Assisted Microwave Processing of Materials. *Energy* **2016**, *97*, 306–338. [CrossRef]
32. Plyler, E.K. Infrared Spectra of Methanol, Ethanol, and n-Propanol. *J. Res. Natl. Bur. Stand.* **1952**, *48*, 281. [CrossRef]
33. Southon, P.D.; Bartlett, J.R.; Woolfrey, J.L.; Ben-Nissan, B. Formation and Characterization of an Aqueous Zirconium Hydroxide Colloid. *Chem. Mater.* **2002**, *14*, 4313–4319. [CrossRef]
34. Phillippi, C.M.; Mazdiyasni, K.S. Infrared and Raman Spectra of Zirconia Polymorphs. *J. Am. Ceram. Soc.* **1971**, *54*, 254–258. [CrossRef]
35. Ayral, A.; Assih, T.; Abenoza, M.; Phalippou, J.; Lecomte, A.; Dauger, A. Zirconia by the Gel Route. *J. Mater. Sci.* **1990**, *25*, 1268–1274. [CrossRef]
36. Arata, K. Organic Syntheses Catalyzed by Superacidic Metal Oxides: Sulfated Zirconia and Related Compounds. *Green Chem.* **2009**, *11*, 1719. [CrossRef]
37. Yadav, G.D.; Nair, J.J. Sulfated Zirconia and Its Modified Versions as Promising Catalysts for Industrial Processes. *Microporous Mesoporous Mater.* **1999**, *33*, 1–48. [CrossRef]
38. Erdey, L.; Gál, S.; Liptay, G. Thermoanalytical Properties of Analytical-Grade Reagents. *Talanta* **1964**, *11*, 913–940. [CrossRef]
39. Kiyoura, R.; Urano, K. Mechanism, Kinetics, and Equilibrium of Thermal Decomposition of Ammonium Sulfate. *Ind. Eng. Chem. Process Des. Dev.* **1970**, *9*, 489–494. [CrossRef]
40. Fernández López, E.; Sánchez Escribano, V.; Panizza, M.; Carnasciali, M.M.; Busca, G. Vibrational and Electronic Spectroscopic Properties of Zirconia Powders. *J. Mater. Chem.* **2001**, *11*, 1891–1897. [CrossRef]

41. Platero, E.E.; Mentruit, M.P. IR Characterization of Sulfated Zirconia Derived from Zirconium Sulfate. *Catal. Lett.* **1995**, *30*, 31–39. [CrossRef]
42. Cerrato, G.; Bolis, V. Lewis and Bronsted Acidity at the Surface of Sulfate- Doped ZrO_2 Catalysts. *Catal. Today* **1993**, *17*, 505–515. [CrossRef]
43. Morterra, C.; Cerrato, G.; Ardizzone, S.; Bianchi, C.L.; Signoretto, M.; Pinna, F. Surface Features and Catalytic Activity of Sulfated Zirconia Catalysts from Hydrothermal Precursors. *Phys. Chem. Chem. Phys.* **2002**, *4*, 3136–3145. [CrossRef]
44. Sarzanini, C.; Sacchero, G.; Pinna, F.; Signoretto, M.; Cerrato, G.; Morterra, C. Amount and Nature of Sulfates at the Surface of Sulfate-Doped Zirconia Catalysts. *J. Mater. Chem.* **1995**, *5*, 353. [CrossRef]
45. Nakamoto, K. *Infrared and Raman Spectra of Inorganic and Coordination Compounds*, 6th ed.; Wiley: Hoboken, NJ, USA, 2009; ISBN 978-0-471-74339-2.
46. Morterra, C.; Cerrato, G.; Pinna, F.; Signoretto, M.; Strukul, G. On the Acid-Catalyzed Isomerization of Light Paraffins over a ZrO_2/SO_4 System: The Effect of Hydration. *J. Catal.* **1994**, *149*, 181–188. [CrossRef]
47. Tsyganenko, A.A.; Filimonov, V.N. Infrared Spectra of Surface Hydroxyl Groups and Crystalline Structure of Oxides. *J. Mol. Struct.* **1973**, *19*, 579–589. [CrossRef]
48. Morterra, C.; Cerrato, G.; Ferroni, L. Surface Characterization of Yttria-Stabilized Tetragonal ZrO_2. Part 3.—CO_2 Adsorption and the CO_2–CO Interaction. *J. Chem. Soc. Faraday Trans.* **1995**, *91*, 125–132. [CrossRef]
49. Morterra, C.; Cerrato, G.; Ferroni, L.; Negro, A.; Montanaro, L. Surface Characterization of Tetragonal ZrO_2. *Appl. Surf. Sci.* **1993**, *65–66*, 257–264. [CrossRef]
50. Bolis, V.; Fubini, B.; Garrone, E.; Morterra, C. Thermodynamic and Vibrational Characterization of CO Adsorption on Variously Pretreated Anatase. *J. Chem. Soc. Faraday Trans. 1 Phys. Chem. Condens. Phases* **1989**, *85*, 1383. [CrossRef]
51. Morterra, C.; Meligrana, G.; Cerrato, G.; Solinas, V.; Rombi, E.; Sini, M.F. 2,6-Dimethylpyridine Adsorption on Zirconia and Sulfated Zirconia Systems. An FTIR and Microcalorimetric Study. *Langmuir* **2003**, *19*, 5344–5356. [CrossRef]
52. McCue, A.J.; Mutch, G.A.; McNab, A.I.; Campbell, S.; Anderson, J.A. Quantitative Determination of Surface Species and Adsorption Sites Using Infrared Spectroscopy. *Catal. Today* **2016**, *259*, 19–26. [CrossRef]
53. Morterra, C.; Cerrato, G.; Meligrana, G. Revisiting the Use of 2,6-Dimethylpyridine Adsorption as a Probe for the Acidic Properties of Metal Oxides. *Langmuir* **2001**, *17*, 7053–7060. [CrossRef]
54. Onfroy, T.; Clet, G.; Houalla, M. Quantitative IR Characterization of the Acidity of Various Oxide Catalysts. *Microporous Mesoporous Mater.* **2005**, *82*, 99–104. [CrossRef]
55. Morterra, C.; Cerrato, G.; Bolis, V.; Di Ciero, S.; Signoretto, M. On the Strength of Lewis- and Bronsted-Acid Sites at the Surface of Sulfated Zirconia Catalysts. *J. Chem. Soc. Faraday Trans.* **1997**, *93*, 1179–1184. [CrossRef]
56. Girisuta, B.; Janssen, L.P.B.M.; Heeres, H.J. Green Chemicals A Kinetic Study on the Conversion of Glucose to Levulinic Acid. *Chem. Eng. Res. Des.* **2006**, *84*, 339–349. [CrossRef]
57. Yan, H.; Yang, Y.; Tong, D.; Xiang, X.; Hu, C. Catalytic Conversion of Glucose to 5-Hydroxymethylfurfural over SO_4^{2-}/ZrO_2 and SO_4^{2-}/ZrO_2–Al_2O_3 Solid Acid Catalysts. *Catal. Commun.* **2009**, *10*, 1558–1563. [CrossRef]
58. Qu, Y.; Zhao, Y.; Xiong, S.; Wang, C.; Wang, S.; Zhu, L.; Ma, L. Conversion of Glucose into 5-Hydroxymethylfurfural and Levulinic Acid Catalyzed by SO_4^{2-}/ZrO_2 in a Biphasic Solvent System. *Energy Fuels* **2020**, *34*, 11041–11049. [CrossRef]
59. Muñoz Tabares, J.A.; Anglada, M.J. Quantitative Analysis of Monoclinic Phase in 3Y-TZP by Raman Spectroscopy. *J. Am. Ceram. Soc.* **2010**, *93*, 1790–1795. [CrossRef]
60. Toraya, H.; Yoshimura, M.; Somiya, S. Calibration Curve for Quantitative Analysis of the Monoclinic-Tetragonal ZrO_2 System by X-ray Diffraction. *J. Am. Ceram. Soc.* **1984**, *67*, C-119–C-121. [CrossRef]
61. Priecel, P.; Lopez-Sanchez, J.A. Advantages and Limitations of Microwave Reactors: From Chemical Synthesis to the Catalytic Valorization of Biobased Chemicals. *ACS Sustain. Chem. Eng.* **2019**, *7*, 3–21. [CrossRef]

Disclaimer/Publisher's Note: The statements, opinions and data contained in all publications are solely those of the individual author(s) and contributor(s) and not of MDPI and/or the editor(s). MDPI and/or the editor(s) disclaim responsibility for any injury to people or property resulting from any ideas, methods, instructions or products referred to in the content.